A bio-inspired optic flow based autopilot for guiding a miniature hovercraft in corridors

Julien Serres, David Dray, Franck Ruffier, and Nicolas Franceschini

Abstract— **Our recent observations on honeybees' flying in an experimental flight tunnel have shown that in addition to the well known 'centering behavior' bees also display 'wall-following' behaviour. We have developed an autopilot, called LORA III, which is inspired by these insect behaviors. It incorporates two interdependent *optic flow (OF) regulators*, each of which controls one translational degree of freedom: a *bilateral OF regulator* controls the robot's speed automatically, while a *unilateral OF regulator* makes the robot avoid the lateral obstacles. Simulation of a fully actuated hovercraft incorporating pair of lateral, OF-sensing eyes show that this robot is able to cross a straight or tapered corridor. This minimalistic visual guidance system suffices to control both speed and clearance from obstacles automatically, without requiring any speed and range sensors. LORA III is a first step toward lightweight and power-lean guidance systems for micro-air vehicles.**

Keywords— OF (optic flow), MAV (micro-air vehicle), hovercraft, indoor navigation, insect flight, bionics, biorobotics.

I. INTRODUCTION

Winged insects are able to navigate swiftly in unfamiliar environments by extracting visual information from their own motion. The *optic flow* (OF) is the apparent motion of the image of contrasting features projected onto the insect's retina. Insects rely on OF to avoid collisions (e.g., [1]), to follow a corridor [2-5], to control their flight speed [6-8], and to cruise and land [8-10], for example.

Kirchner and Srininasan (1989) observed that honeybees flying through a narrow tunnel tend to maintain equidistance from the flanking walls. To explain this 'centering response', these authors hypothesized that the animal may balance the apparent motion of the images of the walls between their two eyes. In the field of robotics, many authors have made use of this 'OF balance' hypothesis in designing visually guided wheeled vehicles, which were tested mainly in corridors and urban canyons [11-17]. Despite the success of this hypothesis in robotics, recent behavioural experiments have shown that honeybees actually do not center systematically when traversing a corridor and may instead follow one wall at a certain distance [3-5]. It remains to be shown whether and how they could generate this behaviour on the basis of OF sensing.

The LORA autopilot described here (LORA stands for Lateral Optic flow Regulation Autopilot) draws on former studies in which we designed the OCTAVE autopilot (OCTAVE stands for Optical flow based Control sysTem for Aerial VEhicles) enabling a Micro-Air Vehicle (MAV) to follow the terrain [10,18]. The LORA autopilot differs from OCTAVE in that it focuses on both issues of automatic speed control and side wall avoidance. We originally developed LORA I, which was a heading control system [19] that could be applied to non-holonomic or underactuated vehicles. We then developed LORA II, which was a forward-plus-side-slip control system based on two OF regulators with a common OF set-point [20] that could be applied to holonomic and fully actuated vehicles. Our latest autopilot, called LORA III, consists of two interdependent OF regulators in which each regulator has its own OF set-point.

The miniature hovercraft we are working on (Fig. 1a) is an advantageous 'MAV' in many ways. It makes no contact with the ground and 'flies' on a plane at a constant height of about 2mm, which eliminates the need to implement an *altitude control system* on-board. A hovercraft is also endowed with inherent roll and pitch stabilization characteristics, which does away with the need to implement an *attitude control system* on-board. LORA III computer-simulated experiments showed its excellent performances in straight and tapered corridors. With both types of corridor, the hovercraft managed to reach a safe forward speed at a safe clearance from the walls.

In section 2, the simulation set-up used to test the LORA III *dual OF regulator* scheme implemented on our *fully actuated* hovercraft is described. In section 3, the LORA III autopilot is described in detail. Section 4 deals with the computer-simulated experiments carried out on the hovercraft equipped with the LORA III autopilot. The results show that LORA III enables the robot to perform various tasks such as *wall-following* and *centring* without having to switch abruptly from one behaviour to the other. It is concluded that the LORA III autopilot provides a simple and lightweight means of guiding a fully actuated air vehicle, while matching the behaviour of honeybees in similar environments.

J. Serres, F. Ruffier, and N. Franceschini are with the Biorobotics Dept. at the Institute of Movement Sciences, CNRS / Uni. of the Mediterranean, CP938, 163 ave. Luminy, 13288 Marseille Cedex 09, France (phone: +33 491 82 83 66; fax +33 491 82 83 75; e-mail: julien.serres@univmed.fr, franck.ruffier@univmed.fr, nicolas.franceschini@univmed.fr).
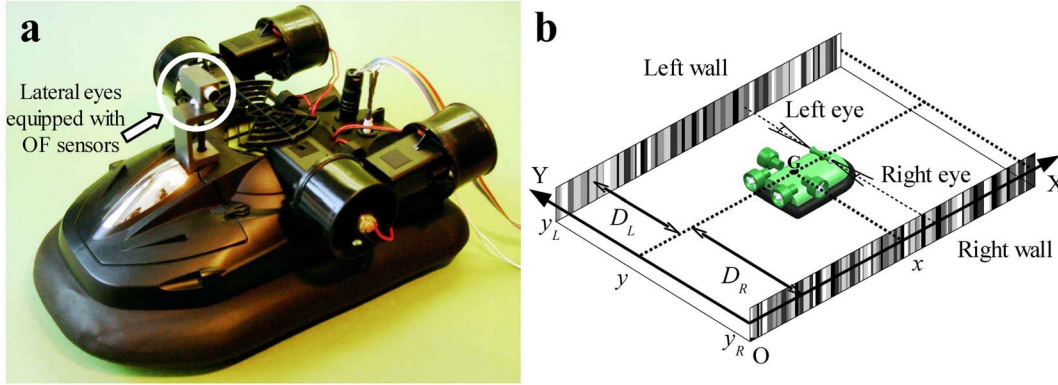
Fig. 1. **a** Sighted fully actuated hovercraft developed for testing the LORA III autopilot. The robot is equipped with two lateral eyes looking at an angle of +90/-90° to the side. Each eye consists of a single OF sensor driven by a pair of PIN photodiodes. **b** Miniature hovercraft moving through an unknown textured corridor. Four thrusters allow the hovercraft to be *fully actuated*, and hence to control the three degrees of freedom in the plane independently. The vehicle's heading ψ is maintained along the X-axis (ψ=0) by means of a heading lock system (e.g., based on a micro magnetic compass) that compensates for any yaw disturbances by acting on the two rear thrusters *differentially* (from [28]).

II. SIMULATION SET-UP

All the present computer-simulated experiments were carried out on a standard PC equipped with the Matlab[TM]/Simulink software program at a sampling frequency of 1kHz.

A. Dynamic hovercraft model

A hovercraft equipped with only two rear thrusters is said to be *underactuated*. Our hovercraft (Fig. 1a), however, is a retrofitted version of a miniature RC hovercraft (Taiyo Toy Ltd., Typhoon T-3: 0.36×0.21×0.14 m). It is *fully actuated* because in addition to the pair of rear thrusters providing forward motion (surge axis) and heading control (yaw axis) (Fig. 1), the vehicle is equipped with a pair of lateral thrusters generating independent side-slip motion (sway axis).

In this study, the hovercraft's heading ψ is assumed to be stabilized along the X-axis of the corridor (ψ =0) by a heading lock system based on a micro magnetic compass (Fig. 1b). Bees are likewise equipped with a heading lock system (based on a polarized light cue, [21]), which makes the insect take an impressively straight course even in the presence of wind [22]. Ethological findings on the behavior of flying insects showed the existence of two distinct visuomotor mechanisms controlling insects' translations and rotations, respectively. The bio-inspired autopilot we designed may explain how a flying insect makes use of its two *translational* degrees of freedom in the plane.

The following linearized system of equations (Eqs. 1) referred to the center of gravity G (Fig. 1b) defines the dynamics of the simulated hovercraft as a function of the four control signals:

$$m.dV_x/dt+ \zeta_x . V_x= K_T.(u_{RT1} + u_{RT2}) \qquad \text{(Eq. 1a)}$$
$$m.dV_y/dt+ \zeta_y . V_y= K_T.(u_{LT2} - u_{LT1}) \qquad \text{(Eq. 1b)}$$

where m is the mass of the hovercraft (platform: 0.70kg + batteries: 0.125kg), and $\zeta_x=\zeta_y$=1.65kg/s are translational viscous friction coefficients along the X-axis and Y-axis, respectively, K_T (0.10 N/V) is a simple gain that relates the thrust to the applied voltage, u_{RT1} and u_{RT2} are the forward control signals received by the rear thrusters (left: RT1 , right: RT2), u_{LT2} and u_{LT1} are the side control signals received by the lateral thrusters (left: LT1, right: LT2).

B. Optic flow generated by the hovercraft's own motion and optic flow measurement

The hovercraft travels at a groundspeed vector $\vec{V}$ over a flat surface along a corridor. The hovercraft is equipped with two lateral eyes placed opposite each other, i.e. looking at $\pm$ 90° to the side. Since any rotations are compensated for (see Section II.A), each eye of the moving platform receives a purely translational OF, which is the relative angular velocity (Eqs. 2) of each stripe on the wall (Fig. 1b). The right and left OF, ω_R and ω_L, respectively, can be simply defined as follows:

$$\omega_R = V_x /D_R \qquad \text{(Eq. 2a)}$$
$$\omega_L = V_x /D_L \qquad \text{(Eq. 2b)}$$

where V_x is the hovercraft's forward speed, D_R and D_L are the distances to the right and the left walls, respectively.

A bio-inspired OF sensor consists of only two photoreceptors (two pixels) driving an Elementary Motion Detector (EMD). The visual axes of the two photoreceptors are separated by an interreceptor angle $\Delta\varphi$=4°. Each photoreceptor angular sensitivity is a bell-shaped function with an acceptance angle (angular width at half height) $\Delta\rho$=4° as well ($\Delta\rho/\Delta\varphi$ = 1). The principle of the EMD circuit used here was derived from electrophysiological experiments performed in the housefly's [23,24] but it does not belong to the "Reichardt correlator" scheme [25]. It is a nonlinear circuit driven by two neighbouring photoreceptors and requiring several processing stages, some of which are realized in a microcontroller [26,27].

$$\text{(Eq. 3a)}$$

III. THE LORA III AUTOPILOT

The LORA III autopilot is based on two interdependent OF regulators (Fig. 2), each of which controls one
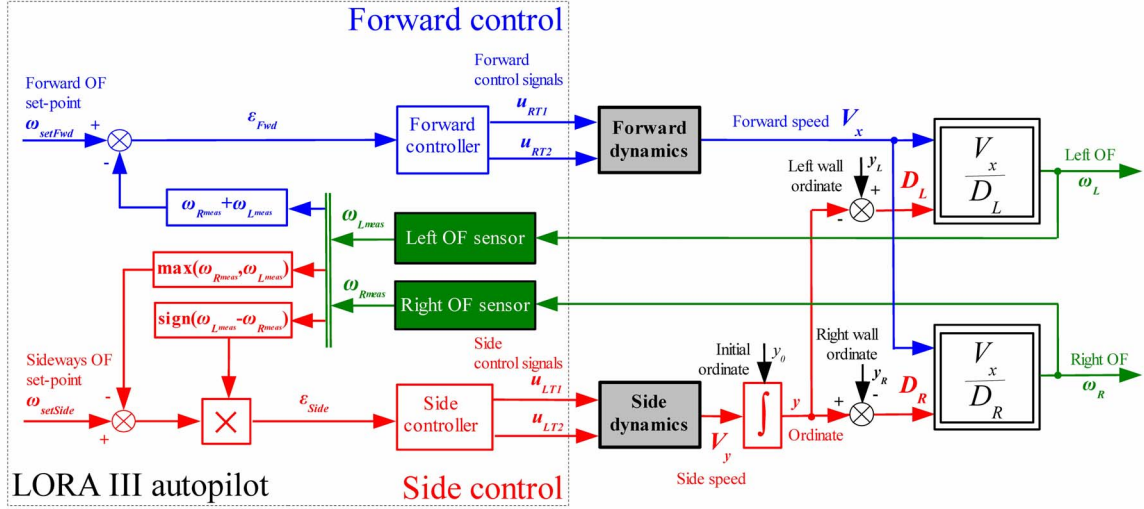
Fig. 2. The LORA III autopilot is based on two visual feedback loops working in parallel with their own optic flow set-point and their own degree of freedom controlled: the forward control system (blue upper loop) and the side control system (red bottom loop). The forward controller adjusts the forward thrust (which determines the hovercraft's forward speed V_x) on the basis of the sum of the right and left OFs measured (green blocks): $\omega_{Rmeas} + \omega_{Lmeas}$. This sum is compared with a forward OF set-point ω_{SetFwd}. The forward controller (PI) commands the forward motion (grey upper block) so as to minimize ε_{Fwd}. The side controller (PD) adjusts the lateral thrust (which determines the hovercraft's side speed V_y, and thus the ordinate y, on the basis of whichever lateral OFs measured is larger. This maximum value is compared with a sideways OF set-point $\omega_{SetSide}$, and the direction of avoidance is given by the sign of the difference between the left and right OFs measured. The side controller commands the side-slip motion (grey bottom block) so as to minimize the error ε_{Side}. The robot's initial ordinate y_0, the right wall ordinate y_R and the left wall ordinate y_L are treated by LORA III like disturbances (black arrows) (from [28]).

translational degree of freedom (X-axis or Y-axis). The *bilateral OF* (Eq. 2a + Eq. 2b) is proportional to the hovercraft's forward speed V_x, and the *bilateral OF regulator* will adjust the forward speed as a function of the corridor width $D = D_R + D_L$ - without actually measuring D. The *unilateral OF* is inversely proportional to the distance, and the *unilateral OF regulator* will adjust the clearance from the *nearer* wall as a function of the forward speed. The tuning procedures for the two controllers is described in detail in [28].

The *bilateral OF regulator* (Fig. 2, blue upper loop) is the forward control system. It is intended to hold the *sum* of the two lateral OFs measured ($\omega_{Rmeas} + \omega_{Lmeas}$) constant and equal to a *forward OF set-point* ω_{SetFwd} by adjusting the forward thrust, which will determine the hovercraft's forward speed V_x. At a given corridor width, any increase in the sum of the two lateral OFs is assumed to result from the hovercraft's acceleration. This control scheme thus automatically ensures a 'safe forward speed', that is, a speed commensurate with the local corridor width. The sum of the two OFs measured is compared with a *forward OF set-point* ω_{SetFwd}, and the error signal ε_{Fwd} (Eq. 3) is calculated as follows:

$$\varepsilon_{Fwd} = \omega_{SetFwd} - (\omega_{Rmeas} + \omega_{Lmeas}) \quad \text{(Eq. 3)}$$

The *unilateral OF regulator* (Fig. 2, red bottom loop) is the side control system. The *unilateral OF regulator* is based on a feedback signal that takes into account the OF provided by the two walls of the corridor. The feedback signal consists of the *larger* of the two OFs measured (left or right), i.e., *max(ω_{Lmeas}, ω_{Rmeas})*, which corresponds to the nearer wall, i.e., *min(D_L, D_R)*. This *OF regulator* was designed to keep the lateral OF constantly equal to a

sideways OF set-point $\omega_{SetSide}$. The hovercraft then reacts to any deviation in the lateral OF from $\omega_{SetSide}$ by adjusting its lateral thrust, which determines the hovercraft's side speed V_y: this eventually leads to a change in the distance to the left (D_L) or right (D_R) wall. A sign function automatically selects the wall to be followed, and a maximum criterion is used to select the higher OF value measured between ω_{Rmeas} and ω_{Lmeas}. This value is then compared with the *sideways OF set-point* $\omega_{SetSide}$ (Fig. 2). The error signal ε_{side} (Eq. 4) feeding the side controller is calculated as follows:

$$\varepsilon_{side} = \text{sign}(\omega_{Lmeas} - \omega_{Rmeas}) \times (\omega_{SetSide} - \text{max}(\omega_{Lmeas}, \omega_{Rmeas}))$$
$$\text{(Eq. 4)}$$

IV. SIMULATION RESULTS

The visual environment simulated here is a 6-meter long *tapered* corridor with a 1.24-meter wide entrance and a 0.5-meter wide constriction located midway (Fig. 3). Its right and left walls are lined with the same random pattern of grey vertical stripes as that used previously (covering a 1-decade contrast range from 4% to 38%, and a 1.5-decade angular frequency range from 0.034 c/° to 1.08 c/° reading from the longitudinal axis of the corridor).

Irrespective of its initial position, the hovercraft can be seen to automatically slow down as it approaches the narrowest section and to accelerate again beyond the constriction (Fig. 3). The hovercraft therefore negotiates a narrow passage by automatically decelerating. In Figure 3, the hovercraft can be seen to adopt a *wall-following behaviour* simply because $\omega_{SetSide} > \omega_{SetFwd}/2$ (see [28]). Figure 3c shows that the forward control system succeeds to keep the sum of the two lateral OFs measured virtually constant
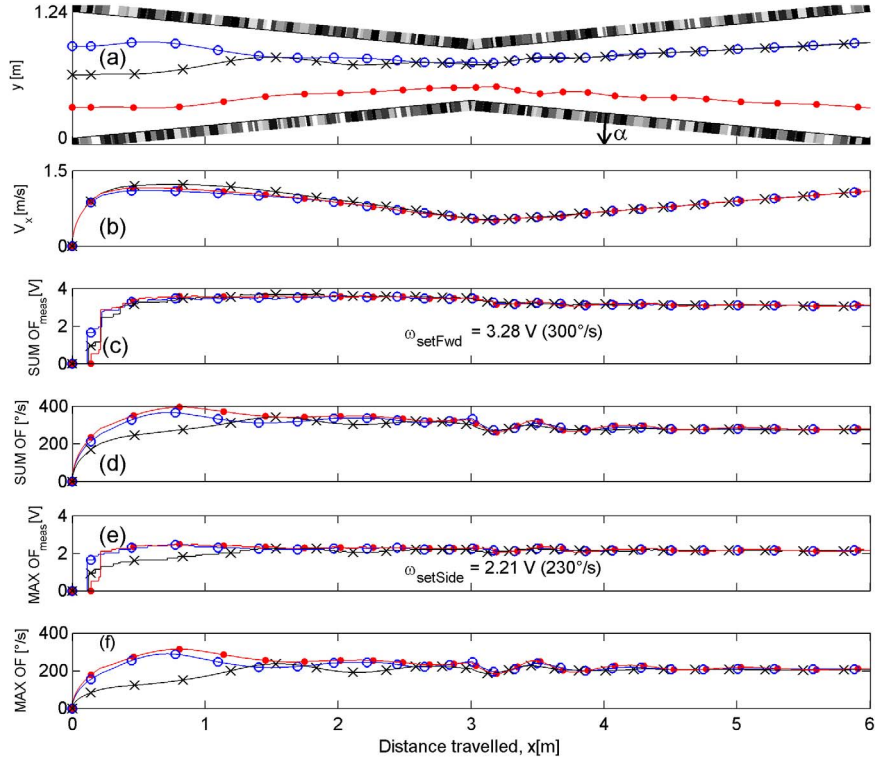
Fig. 3. Automatic deceleration and acceleration of the hovercraft in a tapered corridor in the absence of knowledge on the tapering angle (marks on trajectories indicate the hovercraft position at 0.3-second intervals). **(a)** Three simulated trajectories of the hovercraft moving to the right in a tapered corridor (tapering angle $\alpha = 7°$) at a forward OF set-point ω_{SetFwd} = 3.28V (300°/s) and a sideways OF set-point $\omega_{SetSide}$ =2.21V (230°/s), starting with different initial ordinates (open dots: y_0=0.90m, crosses: y_0=0.60m, full dots: y_0=0.30m). These trajectories show that the hovercraft automatically slows down when the local corridor width decreases and accelerates again when it widens. **(b)** Forward speed profiles corresponding to the three trajectories shown in (a). The forward speed can be seen to be a linear function of the distance x travelled, and it is therefore proportional to the local corridor width D. **(c)** The forward control system strives to maintain the sum of the two lateral OFs measured constant and equal to ω_{SetFwd} = 3.28 V (300°/s). **(d)** Sum of the actual lateral OFs generated by the hovercraft's own motion (computed with Eq. 2a plus Eq. 2b) corresponding to the trajectories shown in (a). The forward control system succeeds to keep the sum of the two lateral OFs measured virtually constant. and equal to 300°/s. **(e)** The side control system strives to keep whichever of the two lateral OFs measured constant and equal to $\omega_{SetSide}$ = 2.21V (230°/s). **(f)** Larger value of the two lateral OFs generated by the hovercraft's own motion (computed with Eq. 2a or Eq. 2b) corresponding to the trajectories shown in (a). The side control system succeeds to keep the larger value of the two lateral OFs virtually constant and equal to 230°/s (from [28]).

and equal to the *forward OF set-point* ω_{SetFwd} = 3.28V (300°/s). Likewise, Figure 3e shows that the side control system itself succeeds to hold the maximum value of the two lateral OFs measured virtually constant and equal to the *sideways OF set-point* $\omega_{SetSide}$ = 2.21V (230°/s). The forward speed profile along the tapered corridor is particularly instructive (Fig. 3b): at all times, the hovercraft's forward speed V_x tends to be proportional to the local corridor width D.

V. CONCLUSION

The results of the present computer-simulated experiments show that a hovercraft can navigate safely under visual control along a tapered corridor (as well as a stationary - or nonstationary - straight corridor, see [28]), although it is equipped with an elementary visual system (consisting of only 4 pixels forming two *elementary motion detectors*, see Fig. 1). The great advantage of this visuomotor control system is that it is able to control the forward speed and the distance to the obstacles *without any speed or range sensors*. The robot navigates on the sole basis of two parameters which are the set-points of the dual

OF regulator: a *sideways OF set-point* $\omega_{SetSide}$ and a *forward OF set-point* ω_{SetFwd}, which fully constrain the vehicle's behaviour in a corridor of a given width. By increasing the *forward OF set-point* at a given *sideways OF set-point*, one can change the vehicle's forward speed. By altering the *sideways OF set-point* at a given *forward OF set-point*, one can induce a graceful shift from 'wall-following behaviour' to 'centring behaviour'. On this view, 'centring behaviour' can be said to be a particular case of wall following behaviour, since it will appear only when choosing $\omega_{SetSide} \leq \omega_{SetFwd}/2$.

Our control scheme (Fig. 3) accounts remarkably well for the behaviour observed in bees flying along a stationary or nonstationary corridor [2], or along a tapered corridor [8], despite the minimalistic number of OF sensors with which it is equipped (one on the right, one on the left). The simulated control scheme described here (Fig. 3) yields data that are similar to those measured in real flying insects [2-5,8], suggesting that a similar control scheme may well be implemented in the insect nervous system.

In terms of applications, a LORA III autopilot would provide the vehicle on which it is mounted with both a speed control system and a lateral obstacle avoidance system. LORA III could be applied to vehicles in which the surge and sway dynamics are uncoupled such as MAVs (e.g.: conventional, coaxial, or quadrotor mini-helicopters).

Insect-based visuomotor control systems can yield solutions requiring a much smaller number of pixels than those used in present-day computer-vision systems harnessed to mobile robots. The LORA III autopilot presented here may open the way to lightweight and low-cost visual guidance systems for autonomous vehicle navigation in unfamiliar indoor environments, as well as in urban canyons where GPS signals may be considerably attenuated by the presence of buildings. The nonemissive OF sensors and the simple processing system described here are particularly suitable for use on MAVs, whose small size imposes draconian constraints on avionic payload and onboard energy resources.

REFERENCES

[1] L.F. Tammero and M.H. Dickinson, "The influence of visual landscape on the free flight behavior of the fruit fly *drosophila melanogaster*," *J. of Exp. Biol.*, vol. 205, pp. 327-343, 2002.

[2] W.H. Kirchner and M.V. Srinivasan, "Freely flying honeybees use image motion to estimate object distance," *Naturwissenschaften*, vol. 76, pp. 281-282, 1989.

[3] F. Ruffier, J. Serres, G.P. Masson, and N. Franceschini, "A bee in the corridor: regulating the optic flow on one side," In *Proc. of the 7th meeting of the German neuroscience society - 31st Göttingen neurobiology conference*, Göttingen, Germany, T14-8A, 2007.

[4] J. Serres, F. Ruffier, G.P. Masson, and N. Franceschini, "A bee in the corridor: centering or wall-following?" In *Proc. of the 7th meeting of the German neuroscience society - 31st Göttingen neurobiology conference*, Göttingen, Germany, T14-8B, 2007.

[5] J. Serres, G.P. Masson, F. Ruffier, and N. Franceschini, "A bee in the corridor: centering and wall-following", *Naturwissenschaften*, 2008 (in rev).

[6] C. David, "Compensation for height in the control of groundspeed by *Drosophila* in a new 'barber pole' wind tunnel," *J. of Comp. Physio.* A, vol. 147, no. 4, pp. 485-493, 1982.

[7] R. Preiss, "Motion parallax and figural properties of depth control flight speed in an insect," *Biol. Cyb.*, vol. 57, pp. 1-9, 1987.

[8] M.V. Srinivasan, S.W. Zhang, M. Lehrer, and T.S Collett, "Honeybee navigation. en route to the goal: visual flight control and odometry," *J. Exp. Biol.*, vol. 199, pp. 237-244, 1996.

[9] E. Baird, M.V. Srinivasan, S. Zhang, and A. Cowling, "Visual control of flight speed in honeybees," *J. Exp. Biol.*, vol. 208, pp. 3895-3905, 2005.

[10] N. Franceschini, F. Ruffier, and J. Serres, "A bio-inspired flying robot sheds light on insect piloting abilities," *Current Biology*, vol. 17, pp. 329-335, 2007.

[11] D. Coombs and K. Roberts, "Bee-bot: using peripheral optical flow to avoid obstacle," in SPIE: *Intelligent robots and computer vision XI*, vol. 1825, pp. 714-721, 1992.

[12] A.P. Duchon and W.H. Warren, "Robot navigation from a Gibsonian viewpoint," in *Proc. Int. Conf. Syst. Man and Cyb.*, pp. 2272-2277, San Antonio, Texas, 1994.

[13] J. Santos-Victor, G. Sandini, F. Curotto, and S. Garibaldi, "Divergent stereo in autonomous navigation: from bees to robots," *Int. J. of Comp. Vision*, vol. 14, pp. 159-177, 1995.

[14] K. Weber, S. Venkatesh, and M.V. Srinivasan, "Insect inspired behaviours for the autonomous control of mobile robots, " in M.V. Srinivasan and S. Venkatesh (Eds), *From living eyes to seeing machines, Oxford: Oxford University Press,* 1997.

[15] A.A. Argyros, D.P. Tsakiris, and C. Groyer, "Biomimetic centering behavior for mobile robots with panoramic sensors," *IEEE Robotics and Automation Magazine*, special issue on "Panoramic Robotics", Eds. K. Daniilides and N. Papanikolopoulos, vol. 11, pp. 21-30, 2004.

[16] S.E. Hrabar, P.I. Corke, G.S. Sukhatme, K. Usher, and J.M. Roberts, "Combined optic-flow and stereo-based navigation of urban canyons for a UAV," In *Proc. of the IEEE/RSJ Int. Conf. on Intelligent Robots and Systems* (Edmonton, Canada) pp. 3309-3316, 2005.

[17] J.S. Humbert, A. Hyslop, and M. Chinn, "Experimental validation of wide-field integration methods for autonomous navigation, " In *Proc. IEEE Int. Conf.Intelligent Robots and Systems* (San Diego, USA) 2007.

[18] F. Ruffier and N. Franceschini, "Optic flow regulation: the key to aircraft automatic guidance," *Robotics and Autonomous Systems*, vol. 50(4), pp. 177-194, 2005.

[19] J. Serres, F. Ruffier, S. Viollet, and N. Franceschini, "Toward optic flow regulation for wall-following and centring behaviours," *Int. J. of Advanced Robotic Systems*, vol. 3, pp. 147-154, 2006.

[20] J. Serres, F. Ruffier, and N. Franceschini, "Two optic flow regulators for speed control and obstacle avoidance," In *Proc. of the first IEEE Int. Conf. on Biomedical Robotics and Biomechatronics* (BIOROB), (Pisa, Italy), pp. 750- 757, 2006.

[21] K. von Frisch, "Gelöste und ungelöste Rätsel der Bienensprache," *Naturwissenschaften*, vol. 35, pp. 38-43, 1948.

[22] J.R. Riley, et al. , "The Automatic Pilot of Honeybees," *Proc. Roy. Soc. Lond.*, vol. 270,pp. 2421-2414, 2003.

[23] C, Blanes, "Appareil visuel élémentaire pour la Navigation à vue d'un robot mobile autonome," M.S. Thesis in Neurosciences ("DEA" in French), Neurosciences, Univ. Aix-Marseille II, 1986.

[24] N. Franceschini, C. Blanes, and L. Oufar, "Passive, non-contact optical velocity sensor," Technical report (in French), France: ANVAR/DVAR N°51549, Paris, 1986.

[25] M. Pudas, S.Viollet, F. Ruffier, A. Kruusing, S. Amic, S. Leppävuori, and N. Franceschini, "A miniature bio-inspired optic flow sensor based on low temperature co-fired ceramics (LTCC) technology," *Sensors and Actuators A*, vol.133, pp.88-95, 2007.

[26] W. Reichart, "Mouvement perception insects," In book: Processing of Optical Data from Organisms and by Machines, W. Reichart (Ed.), NY: Academic Press, 1969.

[27] F. Aubépart and N. Franceschini, "Bio-inspired optic flow sensors based on FPGA: Application to Micro-Air-Vehicles," *J. of Microprocessors & Microsystems*, vol. 31, pp. 408-419, 2007.

[28] J. Serres, D. Dray, F. Ruffier, and N. Franceschini, "A vision-based autopilot for a miniature air-vehicle: joint speed control and lateral obstacle avoidance," *Autonomous Robot*, vol. 25 pp. 103 -122, 2008.